Nanoscale

Accepted Manuscript

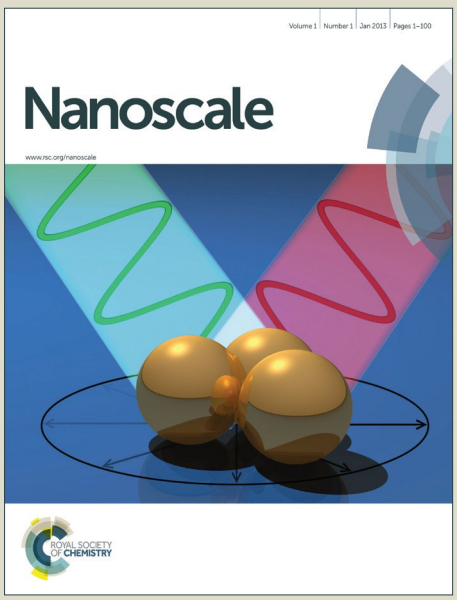

ROYAL SOCIETY OF CHEMISTRY

www.rsc.org/nanoscale

Nanoscale

COMMUNICATION

Exciton and charge carrier dynamics in few-layer WS_2

Victor Vega-Mayoral[a]†, Daniele Vella[a], Tetiana Borzda[a], Matej Prijatelj[a], Iacopo Tempra[b], Eva A. A. Pogna[b], Stefano Dal Conte[b], Peter Topolovsek[c], Natasa Vujicic[d], Giulio Cerullo[b], Dragan Mihailovic[e] and Christoph Gadermaier[a]†.

Received 00th January 20xx,
Accepted 00th January 20xx

DOI: 10.1039/x0xx00000x

www.rsc.org/

Semiconducting transition metal dichalcogenides (TMDs) have been applied as the active layer in photodetectors and solar cells, displaying substantial charge photogeneration yields. However, their large exciton binding energy, which increases with decreasing thickness (number of layers), as well as the strong resonance peaks in the absorption spectra suggest that excitons be the primary photoexcited states. Detailed time-domain studies of the photoexcitation dynamics in TMDs exist mostly for MoS_2. Here, we use femtosecond optical spectroscopy to study the exciton and charge dynamics following impulsive photoexcitation in few-layer WS_2. We confirm excitons as the primary photoexcitations and find that they dissociate into charge pairs with a time constant of about 1.3 ps. The better separation of the spectral features compared to MoS_2 allows to resolve a previously undetected process: these charges diffuse through the samples and get trapped at defects, such as flake edges or grain boundaries, causing an appreciable change of their transient absorption spectra. This finding opens the way to further studies of traps in TMD samples with different defect content.

Semiconducting transition metal dichalcogenides (TMDs) emerge as alternative active materials for applications in electronics, photovoltaics, and photonics, as has been demonstrated by the realization of nanoscale field-effect transistors (FETs), [1] integrated circuits, [2] photovoltaic elements,[3-8] photodetectors,[9] light emitting transistors,[10] and nanoscale lasers.[11] For the design and optimization of such devices it is crucial to understand the non-equilibrium behavior of electrons. Strongly bound excitons (electron-hole pairs with binding energies up to 1 eV) are considered to be the primary photoexcited species in TMDs, and their subsequent dissociation generates the charge carriers necessary for photodetectors and solar cells.[12] Both for applications as well as for basic photophysics, the best studied TMD by far is MoS_2. However, other compounds may be better attuned to certain practical uses or better suited to reveal the underlying photoexcitation dynamics. In femtosecond optical spectroscopy of MoS_2, both excitons and charges show crowded spectra with multiple photobleaching and photoinduced absorption peaks. The close proximity of the A and B exciton features (corresponding to the transition at the K point from the split valence band, due to spin-orbit coupling, to the conduction band) leads to a strong spectral congestion and makes it difficult to untangle the contributions of the individual species. WS_2 shows similar peak widths with about twice the A-B energy separation, [13] which should enable to resolve previously undetected relaxation processes.

The spectral signatures of excitons and charge carriers in TMDs have been identified by absorption and fluorescence spectroscopy, where the charge concentration is varied either via the gate voltage in a FET geometry,[14] via adsorption[15, 16] or substrate doping,[17] or via photoexcitation.[12, 18, 19] The absorption peaks of charges are red-shifted by about 40 meV compared to the ground state absorption into the A and B excitons and have been attributed to optical transitions from a charged ground state to a charged exciton (trion). Recently, in few-layer MoS_2, photoinduced absorption peaks arising from photoexcited charges originating from exciton dissociation have been identified at the same wavelengths. [12]

Here we use femtosecond (fs) optical pump-probe spectroscopy to track the dynamics of photoexcited excitons and charge carriers in few-layer WS_2 flakes obtained by liquid phase exfoliation [20] and redispersed in poly(methyl methacrylate) (PMMA). The sample is photoexcited by a fs laser pulse (the pump) with a photon energy of

[a] Department of Complex Matter, Jozef Stefan Institute
Jamova 39, 1000 Ljubljana, Slovenia
Jozef Stefan International Postgraduate School
Jamova 39, 1000 Ljubljana, Slovenia
[b] IFN-CNR, Department of Physics, Politecnico di Milano, P. Leonardo da Vinci 32, 20133 Milan, Italy
[c] Center for Nano Science and Technology, Italian Institute of Technology
Via Pascoli 70/3, 20133 Milano, Italy.
Jozef Stefan International Postgraduate School
Jamova 39, 1000 Ljubljana, Slovenia.
[d] Institute of Physics
Bijenicka 46, 10000 Zagreb, Croatia
[e] Department of Complex Matter, Jozef Stefan Institute
Jamova 39, 1000 Ljubljana, Slovenia
Jozef Stefan International Postgraduate School
Jamova 39, 1000 Ljubljana, Slovenia
Center of Excellence in Nanoscience and Nanotechnology, Jamova 39, 1000 Ljubljana, Slovenia
† Corresponding author.
See DOI: 10.1039/x0xx00000x

3.1 eV and a fluence of 200 μJ/cm^{-2} and the transient transmission spectrum is measured with a second (lower intensity and broad band) fs laser pulse (the probe) at a well-defined delay after the pump. The measured signal is the relative change in transmission $\Delta T/T$, where a positive signal means photobleaching due to depopulation of initial and population of final states of an absorptive transition, and a negative signal means photoinduced absorption, i.e. an increased absorption from populated excited states towards higher excited states. Scanning the pump-probe delay allows to follow the evolution of the photoexcited states' populations.

The advantages of using a sample containing an ensemble of flakes dispersed in an electronically inert transparent polymer compared to individual flakes are the ease of fabrication and handling [21] and the possibility to use far-field spectroscopic techniques without the need for high spatial resolution optical microscopy. A similar study on MoS_2 flakes embedded in PMMA showed, [12] among others, that such samples display very similar photoexcitation dynamics to the more commonly studied individual few-layer flakes on a dielectric substrate.[22, 23] Additionally, different solvents for liquid exfoliation and different surfactant concentrations have very little influence on the photoexcitation dynamics in MoS_2 films.[24] Hence the results obtained on few-layer MoS_2 in PMMA can be safely compared to other studies and conclusions drawn from them can be extrapolated to flakes in different environments. By analogy, for WS_2, where very few time-resolved studies yet exist, [25, 26] we propose the flake ensemble in PMMA as a prototype sample for few-layer WS_2.

The extinction spectrum in Fig 1 shows the characteristic A, B, C, and D exciton resonances at 1.97, 2.34, 2.72, and 3.05 eV, respectively. Recently, it has been shown how certain characteristics of the extinction spectrum of MoS_2 flakes dispersed in water + sodium cholate and size-selected by centrifugation can serve as a metric to determine the characteristic flake thickness and lateral size.[27] An analogous metric has subsequently been developed for WS_2.[28]

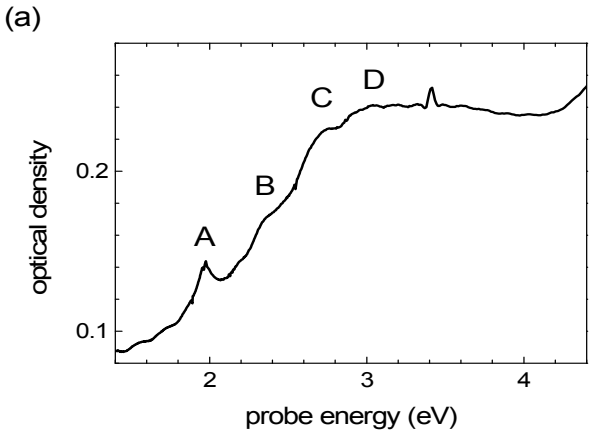

Figure 1. Extinction spectrum of few-layer WS_2 in PMMA. The different exciton absorption resonances are labeled from A to D.

From the A exciton position and the ratio of the A exciton resonance and the absorbance minimum around 4.2 eV, we obtain an average thickness of 7 layers and a characteristic lateral size of 200 nm (along the longer axis, with an average in-plane aspect ratio of 2). Please note that our samples are not as narrowly size selected as those in Refs [27, 28] and hence contain a rather broad distribution of flake sizes, reaching far below 100 nm.

The femtosecond ΔT/T spectra show photobleaching (an increased transmission, Fig 2a) at the A, B, and C excitonic resonances superimposed on a structured photoinduced absorption that covers the whole measured spectral range (1.65-2.8 eV). During the first 10 ps the $\Delta T/T$ spectrum undergoes a characteristic change of shape: the positive signal components, which are formed within the instrumental resolution of ≈100 fs, decay monotonically, while the main photoinduced absorption features show an initial instrument-limited rise followed by a delayed rise component and by a slower decay (See Fig 2b, inset).

We now present a model that relates the evolution of the $\Delta T/T$ spectra to the photoexcitation dynamics. According to Beer-Lambert's law, the transmittance through the sample is:

$$T = exp(-\alpha(\omega)d) \quad (1)$$

With $\alpha(\omega)$ the frequency-dependent absorption coefficient and d the sample thickness. It can easily be shown that, for $\Delta T/T << 1$:

$$\frac{\Delta T}{T} = -\Delta\alpha(\omega, t)d \quad (2)$$

Writing the absorption coefficient $\alpha(\omega) = n\sigma(\omega)$ as the product of the density of absorbers n (i.e. the density of electrons available for an absorptive transition) times their absorption cross section $\sigma(\omega)$, we obtain for $\Delta\alpha(\omega,t)$:

$$\Delta\alpha(\omega, t) = \sum_i(\sigma_i(\omega)\Delta n_i(t) + n_i(t)\Delta\sigma_i(\omega, t)) \quad (3)$$

With the index i denoting the ground state and the various excited state populations. The first term reflects the photoinduced changes in the populations. The second term represents changes in the absorption spectra as a consequence of photoexcitation, such as band gap renormalization,[29] the Burstein-Moss effect[30] or Stark effect due to photoexcited charges.[31-33] All these effects are population dependent, so that the time dependence of $\sigma_i(\omega,t)$ also follows the time dependence of the photoexcited populations. In many cases the second term is either negligible or – since it has the same time dependence as Δn – indistinguishable from a contribution to the first term, and the data can be modeled without the second term.[34] Recently, however, the $\Delta T/T$ spectrum of monolayer MoS_2 300 fs after photoexcitation has been modeled inferring a shift of the ground state absorption as a consequence of band gap renormalization as a main contribution to the signal.[29] Such a shift results in a derivative-shaped spectrum where positive

and negative peaks have a common origin and should show the same time evolution.

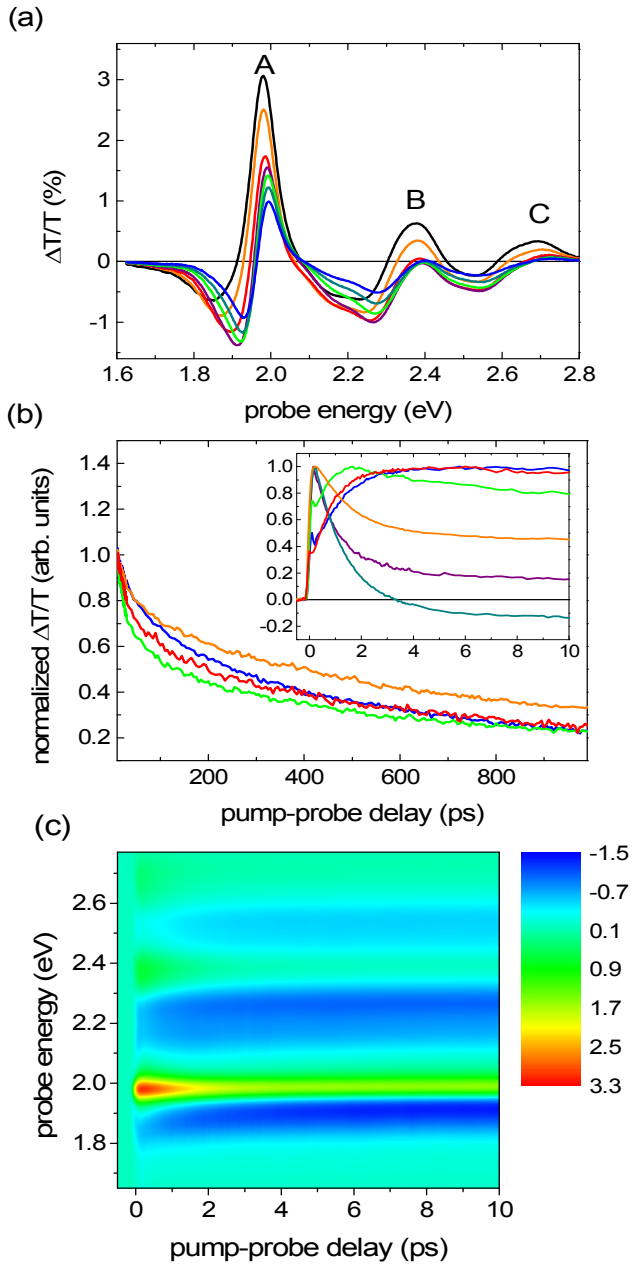

Figure 2. (a) *ΔT/T* spectra of WS_2 in PMMA at delays 300 fs (black), 1 ps (orange), 3 ps (red), 10 ps (purple), 30 ps (green), 100 ps (dark cyan), and 300 ps (blue). (b) Normalized time traces for different probe energies: 1.88 (red), 1.98 (orange), 2.15 (green), 2.52 (blue) in the main figure; the same energies plus 2.37 (dark cyan) and 2.69 eV (purple) in the inset. Traces are normalized to +1 at 10 ps in the main figure and to maximum +1 in the inset. (c) Contour plot of the measured *ΔT/T* (in %).

As shown in Fig 2b, in our case the bleaching peaks form instantaneously, while the absorption peaks show a delayed rise, suggesting they originate from two distinct photoexcited populations. The same behavior in few- layer MoS_2 has been modelled using only the first term of Equation 3, and the second term has been estimated to contribute less than 20% to the signal.[12] The photoexcitation dynamics has been modelled by assuming excitons as the primary photoexcitations,[12] which then dissociate into pairs of charges with lifetime τ_1 ($\tau_i=1/k_i$). In turn, the photogenerated charges recombine with a time constant τ_2:

$$\frac{dE(t)}{dt} = G(t) - k_1 E(t) \quad (4a)$$

$$\frac{dC(t)}{dt} = k_1 E(t) - k_2 C(t) \quad (4b)$$

With *E* and *C* being the time-dependent overall exciton (A, B, and C) and charge populations, respectively, and *G*(*t*) the exciton generation term (pump-probe cross-correlation, approximated as a Gaussian pulse shape). Thus, few-layer MoS_2 displays a behavior which is intermediate between conventional semiconductors, where at room temperature photoexcitation directly generates free carriers, and materials, such as organic semiconductors or carbon nanotubes, with high exciton binding energy, for which the exciton dissociation is much less efficient than in few-layer MoS_2.

For WS_2, this remarkably simple model can coarsely reproduce the most salient characteristics of our result using τ_1 = 1.3 ps and τ_2 = 100 ps (Fig 3a, b), but is somewhat unsatisfactory at the details, in particular the first few ps in the range 1.8 – 2.2 eV. We obtain a much better agreement with the experimental data by adding two elements to the model: an intermediate state with population *I*(*t*) between excitons and unbound charges, and a non-exponential recombination of the charges (Fig 3c):

$$\frac{dE(t)}{dt} = G(t) - k_1 E(t) \quad (5a)$$

$$\frac{dI(t)}{dt} = k_1 E(t) - k_2 I(t) \quad (5b)$$

$$\frac{dC(t)}{dt} = k_2 I(t) - r(t) \quad (5c)$$

The non-exponential decay of the charge population denoted *r(t)* could be due to non-geminate (i.e. bimolecular) recombination, in which case $r(t)=\gamma C^2$, or to a distribution of relaxation times (e.g. different times for different flake thicknesses or lateral sizes). The detailed characterization of this mechanism would require measurements at different pump fluences and over a longer temporal window and is beyond the scope of this paper. We find that excitons dissociate into the intermediate state with a time constant of τ_1 = 1.3 ps, which evolves into the final charges with a time constant of τ_2 = 5.5 ps. To fit the non-exponential long time charge relaxation, without any assumptions about the mechanism, we use a stretched exponential function $r(t) \sim \exp(-(\tau/\tau_3)^{\beta})$ with τ_3 = 450 ps and β= 0.3. The spectral contributions, given as oscillator strength in arbitrary units, include both the photoinduced absorption features of excitons and charges (shown as negative oscillator strength in Fig 4a) and their contribution to the bleaching (as positive oscillator strength). Any kind of excited state population

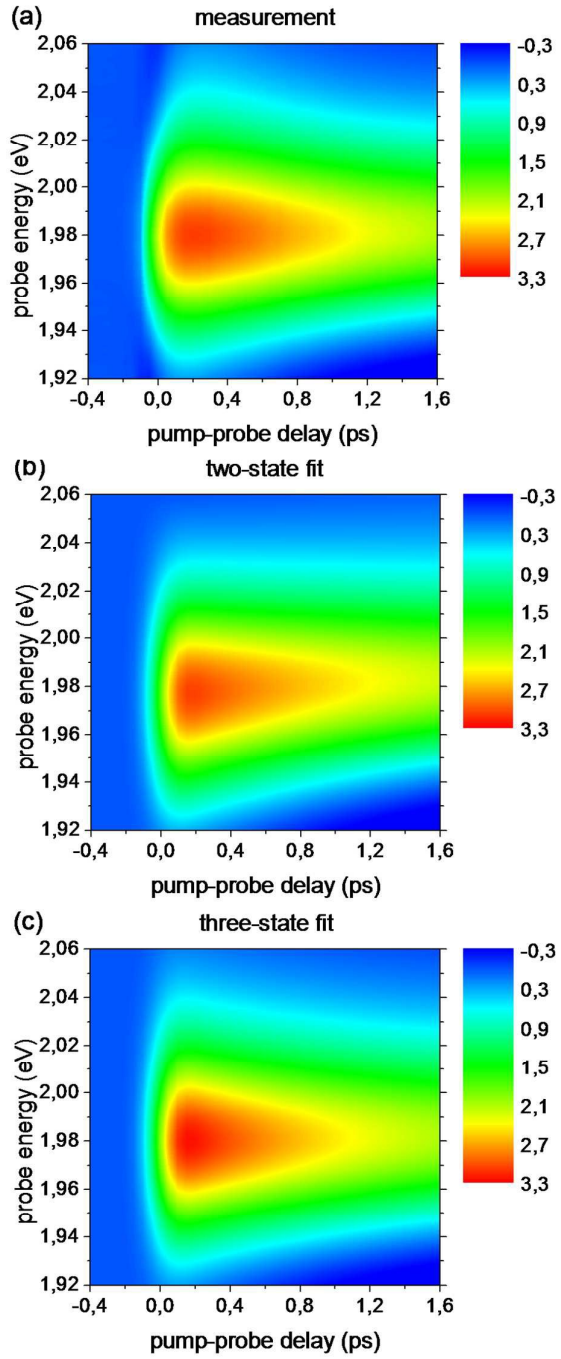

Figure 3. (a) Contour plot of the measured $\Delta T/T$ (in %) around A exciton. (b) Contour plot of the $\Delta T/T$ (in %) fitted with the model of Equations 4a, b. (c) Contour plot of the $\Delta T/T$ (in %) fitted with the model of Equations 5a, b, c.

causes a bleaching of all three exciton peaks in the measured range. Additionally, excitons and charges show several absorption peaks due to transitions towards higher excited states [12, 35-38] (from excitons to higher (two-photon allowed) states and from charges to trions).

The intermediate state spectrum (Fig 4a) deviates from the charges' only slightly, most pronouncedly in the region below 2.3 eV. This similarity suggests that the intermediate states are charges originating from exciton dissociation, but in a different environment than the final charges. For example, upon exciton dissociation, the electrons and hole scatter away from the K points of the direct exciton and relax to their respective band minimum/maximum. However, such relaxation typically occurs on a sub-ps time scale. [39-41] On the other hand, after exciton dissociation, the geminate electrons are still close enough to feel each other's electric field, which can cause Stark shift and/or broadening of their spectra. [31-33]

As they diffuse away from each other, this effect gradually diminishes until the field of the geminate counter-charge becomes a part of the background electric field of the whole charge population. Alternatively, initially free charges may become trapped at defects. Possible such traps are heteroatoms, which are rather common in TMDs of mineral origin, sulfur vacancies, islands of an additional layer, or flake edges. In both cases, τ_2 is a time scale that is associated with diffusion, either with the time it takes a charge to escape its counter-charge or the time to meet a trap.

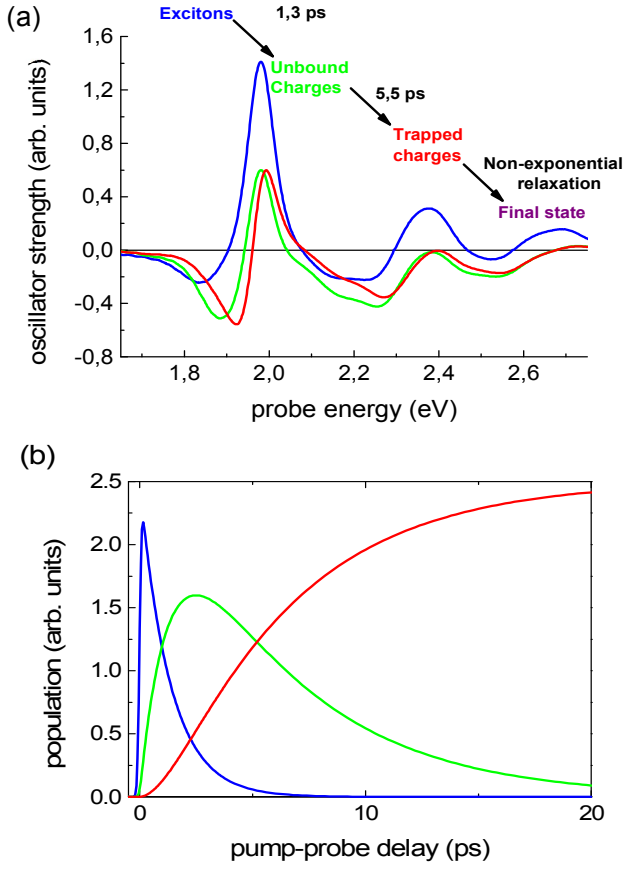

Figure 4. (a) Spectral contributions of excitons (blue), free charges (green), and trapped charges (red). (b) Time dependent exciton (blue), free charge (green), and trapped charge (red) populations.

Assuming that charges follow a random walk after the exciton dissociation we can estimate the diffusion length *l* from τ_2:

$$D = \frac{\mu_e k_B T}{e} \quad (6a)$$

$$l = \sqrt{D\tau_2} \quad (6b)$$

Assuming a conservative estimate of μ_e = 10 cm^2/Vs for the room temperature charge mobility [42] in WS_2, we obtain *D* = 0.25 cm^2/s and *l* = 10 nm. However, the spatially averaged mobility from electrical transport measurement is often dominated by defects and can be much lower than the local mobility probed by femtosecond spectroscopy. For example, in bulk MoS_2 *D* = 18 cm^2/s has been measured over the first 50 ps of the charge recombination, followed by a slower regime of *D* = 4 cm^2/s.[43] Similarly, in monolayer WSe_2 *D* = 15 cm^2/s has been obtained.[44]. However, in the monolayer, exciton dissociation may be less efficient and hence the diffusion constant would be that of excitons rather than charge carriers. Since an exciton would have to scatter as a whole, its scattering cross section may be significantly lower than that of free carriers. Nevertheless, these *D* values, two orders of magnitude higher than in Reference 42, suggest that the diffusion length could be as high as 100 nm. Hence, with our broad distribution of flake sizes centered at 200 nm, flake edges are possible, but not the only candidates for these traps. If we assume that the flake edges trap also excitons, this is consistent with the observed bright fluorescence from the edge of WS_2 monolayer triangles.[45]

Equations 5a-c, which our fit is based on, describe a cascade-like relaxation process, which conserves the overall population of excited states (see Fig 4b), except in the last step (due to the term *-r(t)*). However, we cannot a priori exclude additional processes besides those accounted for in our model, in particular loss mechanisms which do not conserve the excited state population, such as exciton-exciton annihilation or charge recombination. If such losses occur, then our model overestimates all subsequent populations in the cascade, which the fitting procedure compensates by proportionally underestimating the oscillator strength. Exciton dissociation into charges changes the kind of excited species, which have different spectra and oscillator strengths (the blue and green curves in Fig 4a). Trapping of charges, on the other hand, causes only a slight shift in the spectrum and should conserve the oscillator strength. By comparing spectra of free and trapped charges in Fig. 4a, we find that also our fit conserves the oscillator strength and conclude that during the charge migration towards traps or edges no charges are lost by recombination.

The final process that concludes the cascade is charge recombination. If this is the slow decay observed in Fig 2b, then the last term in Equation 5c becomes $r(t)=\gamma C^2$. Since our temporal window is too short to reliably distinguish a quadratic term from the stretched exponential, we used as a generic fit function. A study of this process would require intensity dependent measurements, beyond the scope of the present work.

Exciton-exciton annihilation, which has been observed [46, 47], could be relevant only while there is a significant exciton population, i.e. during the first few ps. Its presence would not have any influence on the qualitative conclusions of the paper nor on the quantitative estimates of the charge mobility and diffusion length.

Conclusions

In conclusion, we have applied femtosecond pump-probe spectroscopy to the study of the exciton and charge dynamics in few-layer WS_2. In agreement with previous observations on TMDs, we find that the primary photoexcitations are excitons which dissociate efficiently with a characteristic time of 1.3 ps. The better separation of the spectral features compared to MoS2 allows to resolve a previously undetected process: The carriers resulting from this dissociation then diffuse randomly away from their counter-charge, which results in a small but appreciable change of the *ΔT/T* spectrum, either due to the diminishing electric field from the countercharge or due to trapping on defects, such as flake edges. This spectral change allows to monitor charge diffusion and trapping in the time domain. The different kinds of defects such as sulfur vacancies, dangling bonds, grain boundaries, or flake edges strongly influence the electronic and optical properties of TMDs [48,49] For example, comparing samples with different flake or crystalline domain sizes can clarify under which circumstances grain boundaries and/or flake edges trap charges. For similar mobilities, shorter τ_2 is expected for the smaller flakes/domains. Different types and densities of defects result from the many methods of synthesizing and exfoliating TMDs. $1/l^2$ as determined from Equations 6a, b gives a measure of the trap density. Since different defects become active traps at different temperatures, measuring the temperature dependence of both the mobility and the photoexcitation dynamics maps the trap energy landscape and can elucidate their role in the charge transport.

Acknowledgements

We gratefully acknowledge J. Strle for inspiring discussions. The research leading to these results has received funding from the Marie-Curie ITN “MoWSeS”. LASERLAB-EUROPE III (grant agreement no. 284464, EC’s Seventh Framework Programme), the ERC Advanced Grant “Trajectory” and the Graphene Flagship (contract no. CNECT-ICT-604391). The research was carried out in the context of and the COST “Nanospectroscopy”.

Notes and references

1 B. Radisavljevic, A. Radenovic, J. Brivio, V. Giacometti, A. Kis, *Nat. Nanotechnol.* 2011, **6**, 147.
2 B. Radisavljevic, M.B. Whitwick, A. Kis, *ACS Nano* 2011, **5**, 9934.
3 M. Fontana, T. Deppe, A. K. Boyd, M. Rinzan, A. Y. Liu, M. Paranjape, P. Barbara, *Sci.Rep*. 2013, **3**, 1634.
4 A.Pospischil, M. M. Furchi, T. Mueller, *Nat. Nanotechnol.* 2014, **9**, 257.
5 B. W. H. Bauger, H. O. H. Churchill, Y. F. Yang, P. Jarillo-Herrero, *Nat. Nanotechnol.* 2014, **9**, 262.
6 L. Britnell, R. M. Ribeiro, A. Eckmann, R. Jalil, B. D. Belle, A. Mishchenko, Y.-J. Kim, R. V. Gorbachev, T. Georgiou, S. V.

Morozov, A. N. Grigorenko, A. K. Geim, C. Casiraghi, A. H. Castro Neto, K. S. Novoselov, *Science* 2013, **340**, 1311.
7 C.-H. Lee, G.-H. Lee, A. M. van der Zande, W. Chen, Y. Li, M. Han, Xu Cui, G. Arefe, C. Nuckolls, T. F. Heinz, J. Guo, J. Hone, Ph. Kim., *Nat. Nanotechnol.* 2014, **9**, 676.
8 X. Hong, J. Kim, S.-F. Shi, Y. Zhang, C. Jin, Y. Sun, S.Tongay, J. Wu, Y. Zhang, F. Wang, *Nat. Nanotechnol.* 2014, **9**, 682.
9 O. Lopez-Sanchez, D. Lembke, M. Kayci, A. Radenovic, A. Kis, *Nat. Nanotechnol.* 2013, **8**, 497.
10 R. S. Sundaram, M. Engel, A. Lombardo, R. Krupke, A. C. Ferrari, P. Avouris, M. Steiner, *Nano Lett.* 2013, **13,** 1416.
11 S. F. Wu, S. Buckley, J. R. Schaibley, L. F. Feng, J. Q. Yan, D. G. Mandrus, F. Hatami, W. Yao, J. Vuckovic, A. Majumdar, X. D. Xu, *Nature* 2015, **520**, 69-72.
12 T. Borzda, C. Gadermaier, N. Vujicic, P. Topolovsek, M. Borovsak, T. Mertelj, D. Viola, C. Manzoni, E. A. A. Pogna, D. Brida, M. R. Antognazza, F. Scotognella, G. Lanzani, G. Cerullo, D. Mihailovic, *Adv. Funct. Mater.* 2015, **25,** 3351-3358.
13 W. Zhao, Z. Ghorannevis, L. Chu, M. Toh, C. Kloc, P.-H. Tan, G. Eda, *ACS Nano* 2013, **7**, 791-797.
14 K. F. Mak, K. He, C. Lee, G. H. Lee, J. Hone, T. F. Heinz, J. Shan, *Nat. Mater.* 2012, **12,** 207.
15 S. Mouri, Y. Miyauchi, K. Matsuda, *Nano Lett.* 2013, **13**, 5944.
16 N. Peimyoo, W. H. Yang, J. Z. Zhang, X. N. Shen, Y. L. Wang, T. Yu, *ACS Nano* 2014, **8**, 11320-11329.
17 N. Scheuschner, O. Ochedowski, A. M. Kaulitz, R. Gillen, M. Schleberger, J. Maultzsch, *Phys. Rev. B* 2014, **89**, 125406.
18 A. A. Mitioglu, P. Plochocka, J. N. Jadczak, W. Escoffier, G. L. J. A. Rikken, L. Kulyuk, D. K. Maude, *Phys. Rev. B.* 2013, **88**, 245403.
19 M. Currie, A. D. Hanbicki, G. Kioseoglou, B. T. Jonker, *Appl. Phys. Lett.* 2015, **106**, 201907.
20 J. N. Coleman, M. Lotya, A. O'Neill, Sh. D. Bergin, P. J. King, U. Khan, K. Young, A. Gaucher, S. De, R. J. Smith, I. V. Shvets, S. K. Arora, G. Stanton, H.-Y. Kim, K. Lee, G. Tae Kim, G. S. Duesberg, T. Hallam, J. J. Boland, Jing Jing Wang, J. F. Donegan, J. C. Grunlan, G. Moriarty, A. Shmeliov, R. J. Nicholls, J. M. Perkins, E. M. Grieveson, K. Theuwissen, D. W. McComb, P. D. Nellist, V. Nicolosi, *Science* 2011, **331**, 568.
21 V. Vega-Mayoral , C. Backes, D. Hanlon, U. Khan, Z. Gholamvand, M. O'Brien, G. S. Duesberg, C. Gadermaier, J. N. Coleman, *Adv. Funct. Mater.*, 2015, DOI: 10.1002/adfm.201503863
22 H. Shi, R. Yan, S. Bertolazzi, J. Brivio, G. Bao, A. Kis, D. Jena, H. G. Xing, L. Huang, *ACS Nano* 2013, **7**, 1072.
23 C. Mai, A. Barrette, Y. Yu, Y. G. Semenov, K. W. Kim, L. Cao, K. Gundogdu, *Nano Lett.* 2014, **14**, 202.
24 D. Vella, V. Vega-Mayoral, C. Gadermaier, N. Vujicic, T. Borzda, Topolovsek, M. Prijatelj, I. Tempra, E. A. A. Pogna, G. Cerullo, *J. Nanophton.* 2015, **10**, 012508.
25 C. Mai, Y. G. Semenov, A. Barrette, Y. F. Yu, Z. H. Jin, L. Y. Zao, K. W. Kim, K. Gundogdu, *Phys. Rev. B.* 2014, **90**, 041414.
26 L. Yuan, L. B. Huang, *Nanoscale.* 2015, **7**, 7402-7408.
27 C. Backes, R. J. Smith, N. McEvoy, N. C. Berner, D. McCloskey, H. C. Nerl, A. O'Neill, P. J. King, T. Higgins, D. Hanlon, N. Scheuschner, J. Maultzsch, L. Houben, G. S. Duesberg, J. F. Donegan, V. Nicolosi, J. N. Coleman, *Nature Commun.* 2014, **5**, 4576.
28 C. Backes, B. M. Szydlowska, A. Harvey, S. Yuan, V. Vega-Mayoral, B. R. Davies, P.-L- Zhao, D. Hanlon, E. J. G. Santos, M. I. Katsnelson, W. J. Blau, C. Gadermaier, J.N. Coleman *ACSNano*, 2015, DOI: 10.1021/acsnano.5b07228.
29 E. A. A. Pogna, M. Marsili, D. de Fazio, S. Dal Conte, C. Manzoni, D. Sangalli, D. Yoon, A. Lombardo, A. C. Ferrari, A. Marini, G. Cerullo, D. Prezzi *ACSNano*, 2015, DOI: 10.1021/acsnano.5b06488
30 Q. C. Sun, L Yadgarov, R Rosentsveig, G Seifert, R. Tenne, J. L. Musfeldt, *ACSNano*, 2013, **7**¸3506
31 V. I. Klimov, S. A. Ivanov, J. Nanda, M. Achermann, I. Bezel, J. A. McGuire, A. Piryatinski, *Nature* 2007, **447**, 441.
32 J. Cabanillas-Gonzalez, T. Virgili, A. Gambetta, G. Lanzani, T. D. Anthopoulos, D. M. de Leeuw, *Phys. Rev. Lett.* 2006, **96**, 106601.
33 C. Gadermaier, E. Menna, M. Meneghetti, W. J. Kennedy, Z. V. Vardeny, G. Lanzani, *Nano Lett.* 2006, **6**, 301.
34 J Cabanillas-Gonzalez, G. Grancini, G. Lanzani *Adv. Mater.*, 2011, **23**, 5468-5485.
35 A. Ramasubramaniam, *Phys. Rev. B* 2012, **86**, 115409.
36 T.Cheiwchanchamnangij, W. R. L. Lambrecht, *Phys. Rev. B* 2012, **85**, 205302.
37 M. Yan, L. J. Rothberg, E. W. Kwock, T. M. Miller, *Phys. Rev. Lett.* 1995, **75**, 1992.
38 C. Manzoni, A. Gambetta, E. Menna, M. Meneghetti, G. Lanzani, G. Cerullo, *Phys. Rev. Lett.* 2005, **94**, 207401.
39 D. Kozawa, R. Kumar, A. Carvalho, K. K. Amara, W. Zhao, Sh. Wang, M. Toh, R. M. Ribeiro, A. H. Castro Neto, K. Matsuda, Goki Eda, *Nature Commun.* 2014, **5**, 4543.
40 A. Leitenstorfer, C. Furst, A. Laubereau, W. Kaiser, G. Trankle, G. Weimann, *Phys. Rev. Lett.* 1996, **76**, 1545.
41 T. Ichibayashi, S. Tanaka, J. Kanasaki, K. Tanimura, T. Fauster, *Phys. Rev. B* 2011, **84**, 235210.
42 B. Radisavljevic, A. Kis, *Nature Mater.* 2013, **12**, 815-820.
43 N. Kumar, J. He, D. He, Y. Wang, H. Zhao, *J. Appl. Phys.* 2013, **113**, 133702.
44 Q. Cui, F. Ceballos, N. Kumar, and H. Zhao, *ACS Nano* 2014, **8**, 2970-2976.
45 H. R. Gutierrez, N. Perea-Lopez, A. L. Elias, A. Berkdemir, B. Wang, R. Lv, F. Lopez-Urias, V. H. Crespi, H. Terrones, M. Terrones, *Nano Lett.* 2013, **13**, 3447-3454.
46 L. Yuan, L. Huang, *Nanoscale,* 2015, **7**, 7402-7408.
47 D. Sun, Y. Rao, G. A. Reider, G. Chen, Y. You, L. Brezin, A. R. Harutyunyan, T.F. Heinz, *Nano Lett,* 2014,**14**, 5625-5629.
48 W. Bao, N. J. Borys, C. Ko, J. Suh, W. Fan, A. Thron, Y. Zhang, A. Buyanin, J. Zhang, S. Cabrini, P.D. Ashby, A. Weber-Bargioni, S. Tongay, S. Aloni, D. F. Ogletree, J. Wu, M. B. Salmeron, P. J. Schuck, *Nature Commun*, 2015, **6**, 7993.
49 A. M. van der Zande, P. Y. Huang, D. A. Chenet, T. C. Berkelbach, Y. M. You, G.-H. Lee, T. F. Heinz, D. R. Reichman, D. A. Muller, J. C. Hone, Nat. Mater, 2013, **12**, 554.